Communication: Neutral atom imaging using a pulsed electromagnetic lens

Jamie R. Gardner, Erik M. Anciaux, and Mark G. Raizen

Citation: The Journal of Chemical Physics **146**, 081102 (2017); doi: 10.1063/1.4976986
View online: http://dx.doi.org/10.1063/1.4976986
View Table of Contents: http://aip.scitation.org/toc/jcp/146/8
Published by the American Institute of Physics

Communication: Neutral atom imaging using a pulsed electromagnetic lens

Jamie R. Gardner, Erik M. Anciaux, and Mark G. Raizen
Department of Physics, University of Texas at Austin, 2515 Speedway, Austin, Texas 78712, USA

(Received 26 December 2016; accepted 7 February 2017; published online 22 February 2017)

We report on progress towards a neutral atom imaging device that will be used for chemically sensitive surface microscopy and nanofabrication. Our novel technique for improving refractive power and correcting chromatic aberration in atom lenses is based on a fundamental paradigm shift from continuous-beam focusing to a pulsed, three-dimensional approach. Simulations of this system suggest that it will pave the way toward the long-sought goal of true atom imaging on the nanoscale. Using a prototype lens with a supersonic beam of metastable neon, we have imaged complex patterns with lower distortion and higher resolution than has been shown in any previous experiment. Comparison with simulations corroborates the underlying theory and encourages further refinement of the process. *Published by AIP Publishing.* [http://dx.doi.org/10.1063/1.4976986]

INTRODUCTION

Atom optics, the manipulation and control of atoms, is a relatively new field that has seen rapid advances since the development of laser cooling. Surprisingly, the most basic atom optics element, the atomic lens, is so hindered by aberrations that resolution has not yet approached the diffraction limit. The correction of aberrations is the single most important factor in the performance of the optical microscope and has enabled angstrom resolution in electron microscopes. A breakthrough in aberration-corrected lenses for atoms will enable the realization of a neutral atom microscope with chemical sensitivity and atomic resolution.

Many approaches to neutral atom imaging have produced encouraging results, but so far none has demonstrated the required resolution or flux.[1–3] Pinhole lenses have been used to deposit indium atoms on a silicon substrate with 30 nm resolution. Unfortunately, a pinhole lens capable of 30 nm resolution must itself be around 20 nm wide, severely limiting atom flux. Fresnel zone plates have larger apertures but still block large portions of the incident beam.[4–6] Zone plate focusing has recently achieved resolution on the order of 1 μm. Standing light waves, which interact with atoms via the AC Stark effect, are amenable to a variety of shaping and tuning techniques.[7–10] While small-period standing waves have achieved nanoscale features, they are limited to simple geometric patterns and do not constitute a general imaging technique.[11,12] Despite some spherical aberration, large-period standing waves can act as universal lenses. Such systems have focused supersonic He* with resolutions around 4 μm.[9] Clever proposals for low-spherical-aberration standing wave lenses with sub-nanometer resolution—for example, based on coaxial TEM_{01}* "doughnut" modes—have yet to fulfill their promise.[2,13] Static dipole forces—electric or magnetic—offer yet another option as atomic lenses. While quadrupole fields have been used,[14,15] the hexapole field is particularly appropriate, since it produces the correct field profile over a large region. Electrodes, permanent magnets, and current-carrying wires have all been employed to create focusing fields.[15–17] A permanent magnet hexapole was used to image a complex mask using slowed Cs atoms ($v = 0–200 \pm 5$ m/s).[18] In addition to their low refractive power, the performance of permanent magnet hexapoles is limited by chromatic aberration. This arises because faster atoms, which require a larger focusing impulse, instead receive a smaller one due to spending less time in the field. The resulting quadratic dependence of focal length on velocity limits the spot size achievable by a steady-state lens.

We propose a pulsed electromagnetic hexapole lens as a solution to the problems of low refractive power, fringing fields, and chromatic aberration.[19] Modern power semiconductor technology in the form of the insulated gate bipolar transistor (IGBT) provides a means for switching large currents ($\geq$1000 A) on microsecond time scales. This allows for high-current wires to exert a brief, strong focusing field on a beam, taking advantage of the high refractive power from current carrying wires without subjecting the atoms to fringing fields as they enter and leave the lens. The pulsed configuration also converts the focal length into a linear function of velocity, since the time spent in the focusing field is fixed for all particles. Further chromatic aberration correction can be achieved by tapering the lens to be narrower towards the front, thereby applying a stronger field and greater force to the faster atoms near the front of the beam. While the pulsed lens can only accommodate similarly pulsed beams, supersonic valves are a perfectly suited source for atom optics experiments. Since these high brightness sources are already pulsed (often at a very high repetition rate), relatively little flux is lost as compared to the continuous case. In addition to addressing the problems of refractive power and chromatic aberration, the pulsed electromagnet is tunable, allowing the user to zoom or focus the lens by simply changing the current. This is in contrast to many other methods, where a fixed focal length creates a rather limited set of adjustable properties.

In this work, we describe the first working prototype of a pulsed electromagnetic hexapole lens. Using Ne*, we observe true imaging of complex patterns on a size scale smaller than any previous hexapole results. We characterize this system at

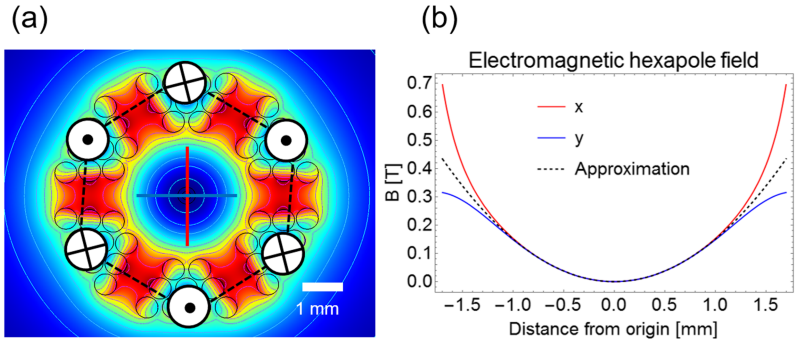

FIG. 1. (a) Schematic of a six-wire hexapole overlaid with a finite-element model depicting the field for a physically realistic wire array. (b) Calculated magnetic field profiles corresponding to traces along the red and blue lines in (a).

a range of focal lengths and observe behavior that compares favorably with theory and simulations. This agreement justifies further exploration of the lens at higher power, where we expect speeds on the order of f/100 and a resolution of 10 nm.[19]

LENS DESIGN

The deflection of paramagnetic atoms in an inhomogeneous magnetic field is based on the same principle as the Stern-Gerlach experiment. For 3^3P_2 metastable neon, $g_j \approx 3/2$. The force exerted by an inhomogeneous magnetic field on an atom in the $m_j = 2$ low-field-seeking (LFS) state is $F \approx -3\,\mu_B \nabla B$. The hexapole field (Figure 1) is a harmonic function of radius ρ, yielding a force that depends linearly on the atomic position. The field from such an object is

$$B(\rho) \cong \frac{6\,\mu_0 I \rho^2}{2\pi R^3}, \tag{1}$$

where I is the wire current and R is the distance of the wires from the axis. The focal length for a collimated atomic disk moving at $v_{||}$ through this pulsed field is

$$f \cong \frac{\pi m v_{||} R^3}{18 \mu_0 \mu_B I \tau}, \tag{2}$$

where m is the mass of a neon atom and τ is the temporal duration of the lens pulse. Note that since $f \propto v_{||}$, atoms with different speeds will focus to different positions. However, this chromatic aberration relation is still an improvement over the steady state lens, since in that case $f \propto v_{||}^2$. The pulsed lens is unique in its ability to deliver a tailored field to each longitudinal segment of the beam. By accounting for both the position and the average velocity of each disk, we can adjust the lens shape to further correct for chromatic aberration. Numerical simulations have shown that tapering the lens will allow us to produce focal spot sizes with 10 nm resolution. In this work, our goal is to build a pulsed hexapole prototype and compare its macro-scale performance with our expectations.

EXPERIMENT

The beamline (Figure 2) begins with a pulsed supersonic nozzle followed by a 3 mm diameter skimmer 17 cm downstream. The supersonic nozzle, connected to ground state neon at 20 bars, is accompanied by a dielectric barrier discharge attachment that excites a fraction of the ground state atoms to the metastable 3^3P_2 state. Following the skimmer, the pulse of Ne* atoms has a divergence angle of 0.017 radians, a mean velocity of 485 m/s, and a longitudinal temperature of 360 mK. We then further collimate and brighten the beam using standard transverse cooling, along with a chirped longitudinal cooling laser propagating nearly antiparallel to the atomic trajectory. After laser cooling, the atomic bullet has approximate transverse and longitudinal temperatures of 2 mK and 10 mK, respectively. In practice, we observe these changes only as increases of order 10–100× in the flux reaching our detector. We also optically pump the beam to the $m_j = 2$ LFS state. All optical processes use the 640 nm cycling transition between the metastable 3^3P_2 and the 3^3D_3 states. Laser light at this frequency is produced in an extended cavity diode laser stabilized to the required wavelength using Doppler-free absorption spectroscopy with an RF-discharge cell.

Following laser cooling and optical pumping, we pass the Ne* beam through either a set of individually translatable knife edges or a brass slide containing apertures of various shapes, including the letter F and a Texas longhorn. This serves as the object plane for our imaging scheme. Using the knife edges, we are able to produce a vertical slit with an adjustable width and position, which allows for several quantitative evaluations of the lens' performance. The shaped apertures, on the other hand, provide more qualitative tests of true imaging on a range of size scales. After the object plane, the atomic beam propagates 135 cm before entering the pulsed electromagnetic hexapole lens. Immediately in front of the lens, a stainless steel chopper

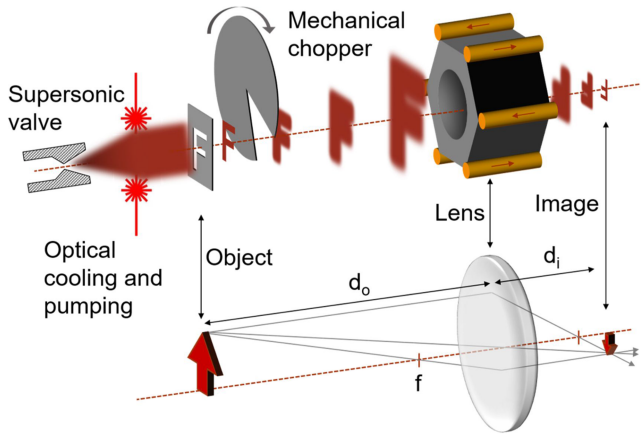

FIG. 2. Schematic image of the experimental sequence for magnetic imaging.

wheel running at 165 Hz with a 3 mm slit reduces the longitudinal extent of the beam to 1 cm. While the atom pulse is entirely within the lens, we pulse a current on the order of 150 A between 25 and 33 μs. We collect data for focal image lengths ranging from 0.6 to 1.1 m. After passing through the magnetic lens, the focused atoms arrive at a microchannel plate (MCP) that serves as the image plane. Metastable atoms arriving at the MCP excite an electron cascade, which is then accelerated towards a phosphor screen. We use a CCD camera to image the phosphor screen through a window in the vacuum chamber. This system allows us to characterize the shape and size of the cross section of the atomic beam where it hits the MCP. Resolution is limited by space charge spreading of the electrons between the MCP and the phosphor screen. Experimental tests with a pinhole have shown the practical resolution limit of this detection system to be around 120 μm.

We construct a prototype lens using a hollow polymer rod (Vespel®, manufactured by DuPont) as a frame to hold a single copper wire wound into the hexapole configuration shown in Figure 1. The rod is connected to a vacuum chamber on both ends using Swagelok hardware. A hole of diameter 1.75 mm drilled along the axis of the rod serves as the lens interior, through which the atoms propagate in a vacuum of order 10^{-7} Torr. The wires are placed approximately 2 mm from the axis. A slight taper is included, but for the focal lengths characterized in this work it is not an important feature. In order to mitigate the effects of stray fields—as well as to counteract any defects arising from imperfect wire placement—we supplement the hexapole with two larger Helmholtz pairs. These coils allow us to empirically smooth the focusing field to obtain better performance. Such measures will likely be unnecessary in future versions of the lens, which will incorporate better background shielding and more precisely placed wires.

RESULTS

We first characterize the performance of the hexapole lens using the adjustable vertical slit formed by two knife edges set 230 μm apart. Placing the image plane at a distance of 61 cm from the lens, we change the lens current (pulsed at $\tau = 33$ μs) until an image comes into focus. The FWHM of the atoms as a function of current is shown in Figure 3(a), from which it is observed that an image forms at around 214 A. From ray optics, we expect the image to have width $w_i = w_o d_i/d_0 \equiv M w_o$, where d_i is the image distance, d_0 is the object distance, w_o is the width of the slit in the object plane, and M is the magnification factor. The detected width of 130 ± 20 μm is near the expected value of 104 μm. This result is particularly close in light of the 120 μm resolution limit of our detection system. Retreating to a longer image distance of 87 ± 2 cm, we obtain a spot size of 150 ± 20 μm at a current of 227 A, pulsed for 25 μs. This agrees rather well with the expected spot size of 147 μm. From our simulations, we expect a lens with R = 2.3 mm, I = 227 A, $\tau = 25$ μs, and $d_0 = 135$ cm to produce an image at 87 cm. Similarly, we expect R = 2.3, I = 227 A, and $\tau = 33$ μs, to yield a spot at $d_i = 62$ cm. This agreement suggests that our simulations accurately describe the important dynamics at work in this system.

To continue analyzing the magnification properties of the lens, we translate the slit horizontally across the object plane by a distance Δx_o. This produces a corresponding shift in the image position, Δx_i, which should obey the simple formula $\Delta x_i = M \Delta x_o$. Repeating this for many values, we obtain a linear relationship from which we can extract a slope. Figure 3(b) shows the data from this process for image distances of 61 ± 2 cm, 87 ± 2 cm, and 113 ± 2 cm. For the first distance, we pulse the lens for 25 μs. For the latter two distances, we pulse for 33 μs. The images at these lengths come into focus at 214 A, 227 A, and 207 A, respectively. The expected magnification factors are 0.45 ± 0.02, 0.64 ± 0.02, and 0.84 ± 0.02. The experimental slopes extracted from the data are 0.42 ± 0.01, 0.63 ± 0.01, and 0.83 ± 0.01. The agreement in these numbers encourages further probing of the lens performance.

A more challenging test for the lens is to image an aperture of a specific size with the correct magnification. This also presents something of a detection challenge, since it is often

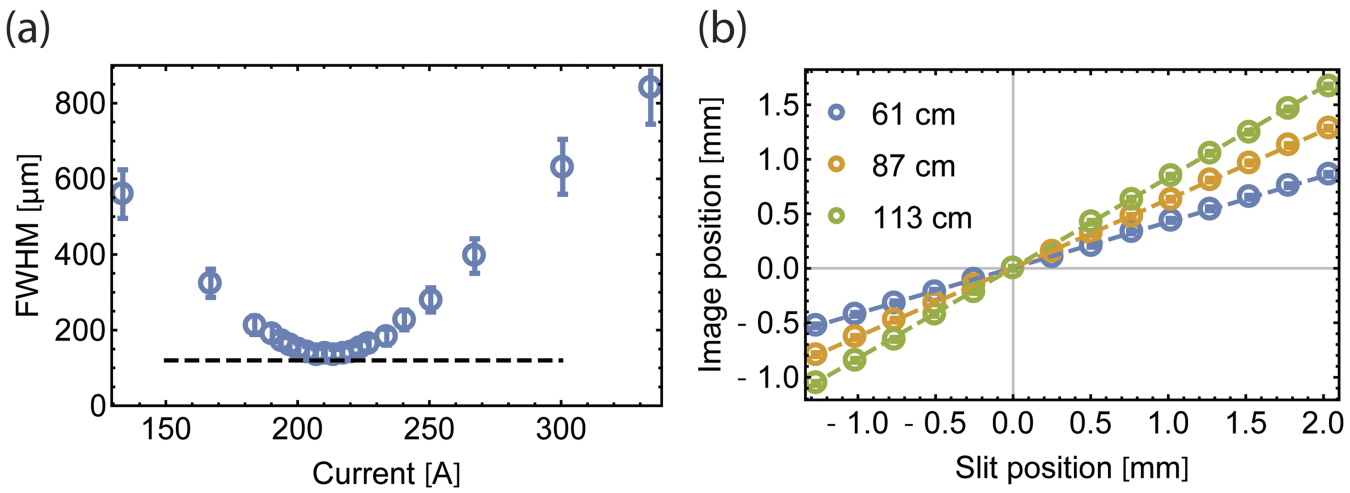

FIG. 3. (a) Width measurement of the image of a vertical slit as a function of lens current, pulsed for 33 μs. The detection plane is placed 61 cm from the center of the lens. The minimum image width occurs at 214 A. The horizontal dashed line at 120 μm represents the resolution limit of the detection system. (b) Image vs. object displacement for image distances of 61 cm, 87 cm, and 113 cm. From the slopes, we extract magnification factors of 0.42 ± 0.01, 0.63 ± 0.01, and 0.83 ± 0.01, respectively.

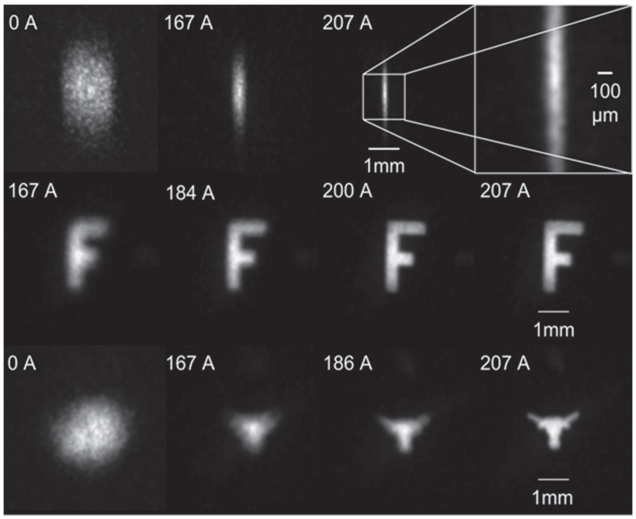

FIG. 4. Image formation using a pulsed hexapole lens. Lens current increases from left to right. The right hand column shows focused images formed by atoms passed through apertures of increasing complexity.

difficult to deconvolve broadening due to imaging aberrations from that arising from the natural resolution limits of our detection system. Nevertheless, the lens performs well, exhibiting a fairly linear regime in which a change in the object size is proportionately matched in the image plane. For all three focal lengths, the linear regime breaks down as the apparent spot size approaches the 120 μm resolution limit of the detector.

Finally, we replace the knife edges with a slide containing various geometric shapes. To minimize the importance of the detector resolution, we look for images at 113 cm, where $M \cong 0.84$. Figure 4 shows three sequences of images produced as the system is brought into focus. The top sequence depicts a slit focusing process analogous to that described in Figure 3(a). At the focus, we observe an image width of 170 ± 20 μm. More interesting than a simple slit is the letter F, which comes into sharp focus in the second sequence at the same current (207 A) that worked for the slit. Though the figure does not show this, the letter appears on the MCP upside-down and backwards, just as ray optics would predict. The bottom sequence features a more complex shape and demonstrates a resolution of detail on the scale of the detection limit. These images show that the pulsed hexapole lens simultaneously reproduces features at both the large and the small scales, which is a crucial feature for many potential applications.

The use of Helmholtz coils to empirically tune the field inside the lens is a crucial component of attaining the resolution shown in Figure 4. Without these coils, the lens produces a characteristic "double image" consistent with either a background magnetic field or slightly asymmetric wire placement. Calculations suggest that correcting these aberrations with an external field is only possible to a finite degree. In order to reach the nanoscale, therefore, both background fields and wire placement error must be minimized. A second-generation lens incorporating the necessary control features is in the design phase.

CONCLUSION

The pulsed, tapered, electromagnetic hexapole represents a fundamentally new approach to chromatic aberration-correction in atom lenses. Simulations suggest that this system can produce images and spots with nanoscale resolution, providing a high quality tool for beam management in atom optics experiments and paving the way for breakthroughs in nanofabrication and surface microscopy. We have demonstrated that our pulsed magnetic lens—the first of its kind—can image a beam of neutral atoms with higher resolution and lower distortion than any previous hexapole system. Close agreement with numerical simulations and the principles of ray optics provides strong encouragement that future generations of this lens will be able to achieve nanoscale atomic focusing.

ACKNOWLEDGMENTS

The authors thank Dr. Rodrigo Castillo-Garza, Georgios Stratis, and Yi Xu and acknowledge the support of R. A. Welch Foundation Grant No. F-1258 and the Sid W. Richardson Foundation.

[1] V. I. Balykin, P. A. Borisov, V. S. Letokhov, P. N. Melentiev, S. N. Rudnev, A. P. Cherkun, A. P. Akimenko, P. Y. Apel, and V. A. Skuratov, JETP Lett. **84**, 466 (2006).
[2] V. I. Balykin and V. S. Letokhov, Opt. Commun. **64**, 151 (1987).
[3] P. N. Melentiev, A. V. Zablotskiy, D. A. Lapshin, E. P. Sheshin, A. S. Baturin, and V. I. Balykin, Nanotechnology **20**, 235301 (2009).
[4] O. Carnal, M. Sigel, T. Sleator, H. Takuma, and J. Mlynek, Phys. Rev. Lett. **67**, 3231 (1991).
[5] T. Reisinger, S. Eder, M. M. Greve, H. I. Smith, and B. Holst, Microelectron. Eng. **87**, 1011 (2010).
[6] S. D. Eder, T. Reisinger, M. M. Greve, G. Bracco, and B. Holst, New J. Phys. **14**, 073014 (2012).
[7] F. Lison, H.-J. Adams, D. Haubrich, M. Kreis, S. Nowak, and D. Meschede, Appl. Phys. B: Lasers Opt. **65**, 419 (1997).
[8] G. Timp, R. Behringer, D. Tennant, J. Cunningham, M. Prentiss, and K. Berggren, Phys. Rev. Lett. **69**, 1636 (1992).
[9] T. Sleator, T. Pfau, V. Balykin, and J. Mlynek, Appl. Phys. B: Photophys. Laser Chem. **54**, 375 (1992).
[10] V. I. Balykin and P. N. Melentiev, Nanotechnol. Russ. **4**, 425 (2009).
[11] W. R. Anderson, C. C. Bradley, J. J. McClelland, and R. J. Celotta, Phys. Rev. A **59**, 2476 (1999).
[12] J. J. McClelland, R. E. Scholten, E. C. Palm, and R. J. Celotta, Science **262**, 877 (1993).
[13] J. J. McClelland and M. R. Scheinfein, J. Opt. Soc. Am. B **8**, 1974 (1991).
[14] M. Mützel, M. Müller, D. Haubrich, U. Rasbach, D. Meschede, C. O'Dwyer, G. Gay, B. V. De Lesegno, J. Weiner, K. Ludolph, G. Georgiev, and E. Oesterschulze, Appl. Phys. B **80**, 941 (2005).
[15] W. Kaenders, F. Lison, I. Müller, A. Richter, R. Wynands, and D. Meschede, Phys. Rev. A **54**, 5067 (1996).
[16] H. R. Noh and F. Shimizu, Phys. Rev. A **61**, 041601 (2000).
[17] H. Friedburg, Z. Phys. **130**, 493 (1951).
[18] W. G. Kaenders, F. Lison, A. Richter, R. Wynands, and D. Meschede, Nature **375**, 214 (1995).
[19] R. Castillo-Garza, J. Gardner, S. Zisman, and M. G. Raizen, ACS Nano **7**, 4378 (2013).